Earth and Planetary Science Letters 457 (2017) 136–148

Contents lists available at ScienceDirect

Earth and Planetary Science Letters

www.elsevier.com/locate/epsl

Hydrological and temperature change in Arctic Siberia during the intensification of Northern Hemisphere Glaciation

Benjamin A. Keisling *, Isla S. Castañeda, Julie Brigham-Grette

Department of Geosciences, University of Massachusetts Amherst, 233 Morrill Science Center, 611 North Pleasant St., Amherst, MA 01002, USA

ARTICLE INFO

Article history:
Received 29 January 2016
Received in revised form 28 August 2016
Accepted 14 September 2016
Available online 25 October 2016
Editor: H. Stoll

Keywords:
arctic
branched GDGT
Northern Hemisphere glaciation
n-alkane hydrogen isotopes
palaeoclimate
Pliocene

ABSTRACT

The Pliocene epoch represents an analog for future climate, with atmospheric carbon dioxide concentrations and continental configurations similar to present. Although the presence of multiple positive feedbacks in polar regions leads to amplified climatic changes, conditions in the Pliocene terrestrial Arctic are poorly characterized. High latitude sedimentary records indicate that dramatic glacial advance and decay occurred in the Pliocene Arctic, with attendant effects on global sea-level. Understanding these deposits and their implications for Earth's future requires developing a sense of climatic evolution across the Pliocene–Pleistocene transition and during the intensification of Northern Hemisphere Glaciation (iNHG) ~2.7 million yr ago (Ma). Here we reconstruct Arctic terrestrial environmental change from 2.82–2.41 Ma (Marine Isotope Stages (MIS) G10–95) using the distribution of branched glycerol dialkyl glycerol tetraethers (brGDGTs) and the isotopic composition of plant leaf waxes (δD_{wax}) in a sedimentary archive from Lake El'gygytgyn, Northeast Russia. Our records reveal changes in proxy behavior across this interval that we attribute to changing boundary conditions, including sea level, sea ice, vegetation and pCO_2 during different MISs. We find that brGDGT temperatures and δD_{wax} are decoupled for most of the record, although both show an increasing range of glacial–interglacial variability following iNHG. δD_{wax} is stable from MIS G10–G4 despite changes in vegetation and temperature, suggesting different sources or pathways for moisture to Lake El'gygytgyn during the Late Pliocene.

1. Introduction

The Pliocene was a global warm period 5.332–2.588 million yr ago (Ma) (Gibbard et al., 2010) when atmospheric carbon dioxide (pCO_2) was 350–450 ppm (Zhang et al., 2013; Martínez-Botí et al., 2015), and it has been proposed as an analog for future warming (Thompson and Fleming, 1996). Of particular interest is the intensification of Northern Hemisphere glaciation (iNHG) ~2.73 Ma, during Marine Isotope Stage (MIS) G6, which has been studied in many high-latitude marine records (Fig. 1) (e.g. Haug et al., 2005; Naafs et al., 2012; Hennissen et al., 2015; Bailey et al., 2013; Kleiven et al., 2002; Martínez-Garcia et al., 2010). Northern landmasses were permanently altered by the growth of large ice sheets after iNHG, yet few terrestrial records from this period have been studied. Unfortunately, high-resolution, continuous terrestrial sections of Pliocene age are rare in the high latitudes. Pleistocene glaciations repeatedly scoured the continents, precluding the uninterrupted deposition of sediment necessary to develop a continuous view of terrestrial Arctic climate change since the Pliocene (Miller et al., 2010).

In 2009, a sediment core from Lake El'gygytgyn, Russia, spanning the last ~3.6 Ma was recovered. This record provides a unique view of environmental change preceding, during, and following iNHG. Although pollen-based temperature estimates have been published for Lake El'gygytgyn (Melles et al., 2012; Brigham-Grette et al., 2013), these are regional in nature and potentially subject to large errors based on the modern analogue approach (Andreev et al., 2014). Organic geochemical proxies provide an independent means of examining terrestrial temperature and hydrological change (e.g. Weijers et al., 2007a; Pautler et al., 2014) and may provide a more local signal in a lacustrine environment (Buckles et al., 2014). Here we apply two such proxies that have previously been used to reconstruct past Arctic temperature from marine and lacustrine sediments (e.g. de Wet et al., 2016; Pautler et al., 2014). Firstly, we use the methylation/cyclization (MBT/CBT) ratio based on branched glycerol dialkyl glycerol tetraethers (brGDGTs) (Weijers et al., 2007b; Peterse et al., 2012). Secondly, we measure the deuterium to hydrogen ratio on terrestrial higher plant leaf waxes (*n*-alkane δ^2H, δD, or δD_{wax}) (e.g. Sachse et al., 2012).

* Corresponding author.
E-mail address: bkeisling@geo.umass.edu (B.A. Keisling).

http://dx.doi.org/10.1016/j.epsl.2016.09.058
0012-821X/

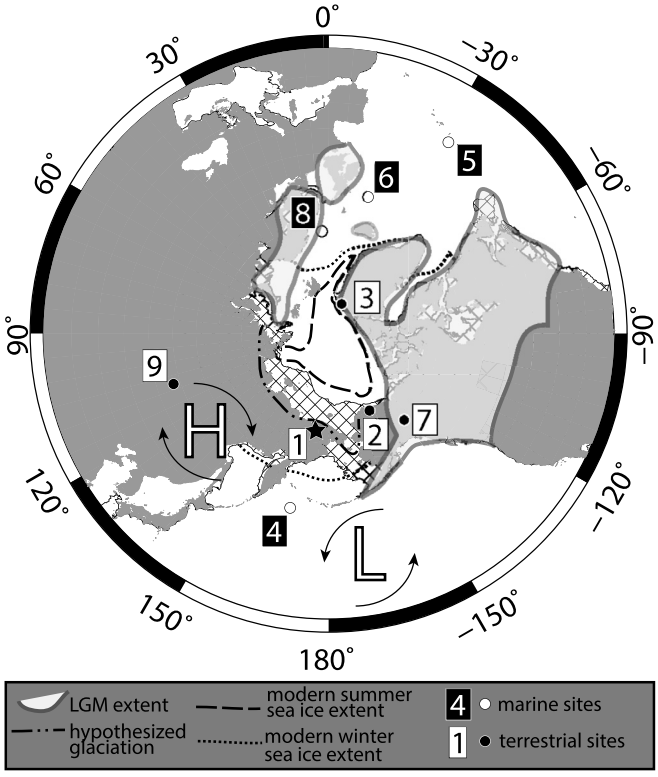

Fig. 1. Lake El'gygytgyn and surrounding records. The dashed black line indicates approximate September sea-ice extent; dotted black line indicates March sea-ice extent (http://neo.sci.gsfc.nasa.gov). The hatched area marks modern seafloor that becomes subaerial during Last Glacial Maximum (LGM) style glaciations (the −120 m bathymetric contour). The transparent gray areas mark the approximate extent of LGM ice sheets; a dotted black line in Siberia from 90–180° longitude marks the hypothesized extent of the East Siberian Ice Sheet, which existed during some Plio-Pleistocene glacial stages (Niessen et al., 2013). Records and localities discussed in the text are marked: (1) Lake El'gygytgyn (this study), (2) Fish Creek (Brigham-Grette and Carter, 1992), (3) Kap København (Funder et al., 2004), (4) ODP 882 (Haug et al., 2005), (5) U1313 (Naafs et al., 2012; Hennissen et al., 2015), (6) ODP 611 (Bailey et al., 2013), (7) Yukon (Duk-Rodkin and Hughes, 1994), (8) Vøring Sea (Kleiven et al., 2002), (9) Lake Baikal. Arrows indicate prevailing winds around the approximate mean position of the Aleutian Low (L) and Siberian High (H).

2. Study area and regional setting

Lake El'gygytgyn is located in northeastern Arctic Russia (67.5°N, 172°E, Fig. 1). A bolide impact created the lake, resulting in a small catchment with a high degree of topographic relief (Layer, 2000; Nolan and Brigham-Grette, 2007). The lake and its catchment are roughly circular, with diameters of ∼12 km and ∼18 km, respectively. The 175-meter deep lake is ice-covered for ∼10 months of the year, with most inflow during the early June freshet, delivered by 50 small creeks around the perimeter (Nolan and Brigham-Grette, 2007).

Lake El'gygytgyn was unscathed by the periodic glaciations of the Plio-Pleistocene, perhaps due to the arid climate of northeast Chukotka (Barr and Clark, 2011). As such, it has accumulated a continuous sedimentary record since its formation (Brigham-Grette et al., 2013). In 2009, the International Continental Scientific Drilling Program recovered 318 m of composite core from the lake (Brigham-Grette et al., 2013; Melles et al., 2012). Three separate drives comprise the composite core, which were correlated based on their lithological properties (Gebhardt et al., 2013). The age model is based on a three-tiered system of tie points: primarily, on twelve magnetic reversals dated by the geomagnetic polarity timescale; secondarily, by tuning the elemental ratio of silica/titanium and hue angle to the benthic oxygen isotope ($\delta^{18}O$) stack of Lisiecki and Raymo (2005); and lastly, by tuning of magnetic susceptibility and percent total organic carbon (%TOC) to Northern Hemisphere summer insolation (Nowaczyk et al., 2013). The uncertainty in absolute age is 3–15 thousand years (kyr), with higher uncertainties during the Pliocene portion of the record (Nowaczyk et al., 2013). Differences in spatial and temporal averaging in sediments of the three proxies used (*n*-alkanes, brGDGTs, and pollen) may account for some of the differences discussed here, and is further explored in the supplementary materials. However, we anticipate these to be minimal as the mean sedimentation rate during our study interval results in each 1-cm thick sample representing ∼300 yr. In addition, measuring proxies (MBT/CBT and δD_{wax}) on the same samples permits observations that are unaffected by changes to the age model.

Lake El'gygytgyn sits between two prominent atmospheric pressure centers in the Northern Hemisphere, the Siberian High and the Aleutian Low (Fig. 1). Although their position and strength show significant interannual variability, their mean position causes extreme windiness at the lake (Fig. 1) (Mock et al., 1998). Aloft, the persistent East Asian Trough in the jet stream brings southerly flow to the lake (Mock et al., 1998). In summer, the Pacific subtropical high sits over the northeastern Pacific, bringing predominately southerly surface flow (Mock et al., 1998). Historical observations of atmospheric circulation patterns are consistent with weather station data spanning 2002, which showed winds were predominantly south-easterly and north-westerly (Nolan et al., 2013). The lake is extremely arid (<200 mm a^{-1}), with precipitation occurring in approximately equal amounts in summer and winter (Nolan and Brigham-Grette, 2007). Although the Siberian High and Aleutian Low are persistent features of the climatology, they are subject to change as the jet stream kinks and migrates, and the mean climatology at the lake may have shifted over time, especially over the long duration of this study. In addition, the imposition of large ice masses in the Northern Hemisphere has dramatic consequences for the atmospheric pressure centers mentioned here. Studies of the Last Glacial Maximum indicate an intensified Aleutian Low, and a potential splitting of the jet stream aloft advecting more southerly-sourced air over Lake El'gygytgyn (Bromwich et al., 2004). In sum, the position of Lake El'gygytgyn makes it sensitive to changes both in the Chukchi Sea and terrestrial Siberia (Fig. 1).

3. Sampling and methods

3.1. Sample preparation

Sediment samples were collected at one-centimeter intervals from the working half of each core section where possible, and the archive half where necessary. For this study, we analyzed samples every ∼10 cm throughout the composite core, resulting in a climate reconstruction with ∼2 kyr resolution from 2.82–2.41 Ma (mean sample spacing = 2.3 kyr, median = 1.3 kyr). Freeze-dried, homogenized samples were extracted using a Dionex accelerated solvent extraction (ASE 200) system with a mixture of dichloromethane (DCM):methanol (9:1, v:v). Total lipid extracts (TLEs) were dried under a stream of N_2 and separated into apolar, ketone, and polar fractions by sequential elution over activated Al_2O_3 using DCM:hexane (9:1, v:v) (apolar), DCM:hexane (1:1, v:v) (ketone), and DCM:methanol (1:1, v:v) (polar).

3.2. brGDGT analysis

One half of each polar fraction was filtered through a 0.45 µm PTFE filter in hexane:isopropanol (99:1, v:v), then dried under a stream of N_2 and dissolved in 100 µl hexane:isopropanol containing 0.1 µg of a C_{46} GDGT internal standard. BrGDGTs were

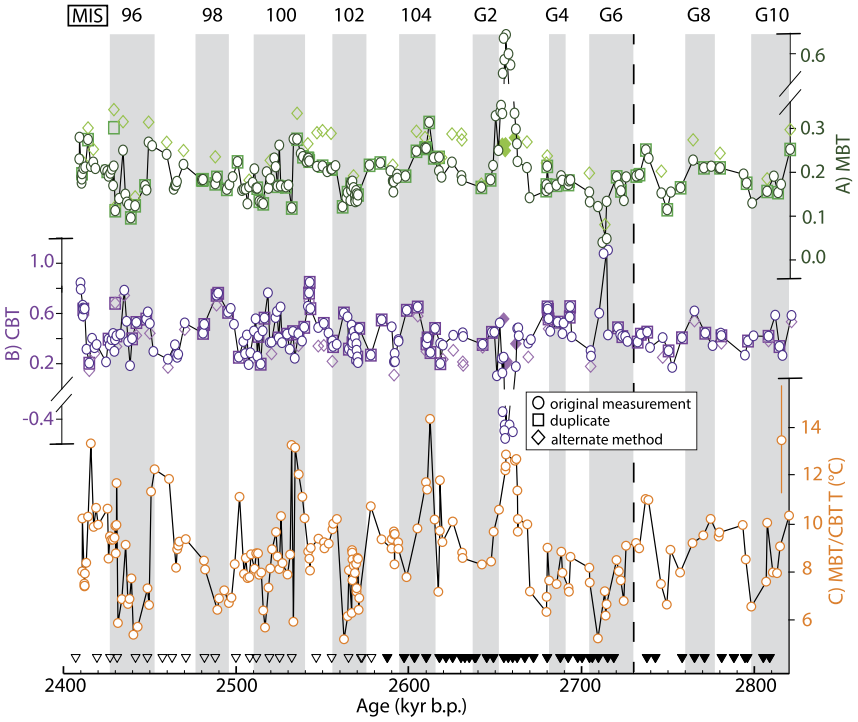

Fig. 2. BrGDGT-based proxies measured on Lake El'gygytgyn sediments. A) Methylation of Branched Tetraethers (MBT), B) Cyclization of Branched Tetraethers (CBT). Circles are the initial measurements, squares show duplicate measurements, and diamonds indicate measurement with a new UHPLC method (Hopmans et al., 2016). C) Temperature reconstruction applying the lacustrine MBT/CBT calibration of Sun et al. (2011). Orange vertical line near the y-axis shows the published calibration error (4.27 °C). Glacial marine isotope stages based on the chronology of Lisiecki and Raymo (2005) are labeled at the top and shaded in gray. The black dashed line indicates the approximate start of iNHG at 2.73 Ma. The triangles indicate second- or third-order age model tie points for the Lake El'gygytgyn core, with solid triangles falling in the Gauss chron (Nowaczyk et al., 2013).

quantified with respect to the C_{46} standard, assuming equal ionization efficiency for all compounds. BrGDGTs were analyzed using an Agilent 1260 High Performance Liquid Chromatograph (HPLC) coupled to an Agilent 6120 Mass Selective Detector (MSD), equipped with a Prevail Cyano column (150 mm × 2.1 mm × 3 µm) run in selected ion monitoring (SIM) mode for the major brGDGT protonated molecules $[M+H]^+$. GDGTs were eluted by 99:1 hexane:isopropanol for 7 min, then by a linear solvent gradient culminating in 1.8% isopropanol after 32 additional minutes (Hopmans et al., 2000; Schouten et al., 2007).

Weijers et al. (2007b) proposed the MBT/CBT proxy for mean annual air temperature (MAAT) based on the distribution of brGDGTs. brGDGTs are comprised of two ether-linked dialkyl chains containing zero to two methyl branches (prefixes I, II, and III) and zero to two cyclopentane moeities (suffixes a, b, and c). Based on the abundance of these structures, Weijers et al. (2007b) developed the MBT (methylation of branched tetraethers) and CBT (cyclization of branched tetraethers) indices.

$$MBT = \frac{[\mathbf{Ia}+\mathbf{Ib}+\mathbf{Ic}]}{[\mathbf{Ia}+\mathbf{Ib}+\mathbf{Ic}]+[\mathbf{IIa}+\mathbf{IIb}+\mathbf{IIc}]+[\mathbf{IIIa}+\mathbf{IIIb}+\mathbf{IIIc}]} \quad (1)$$

$$CBT = -log\frac{[\mathbf{Ib}]+[\mathbf{IIb}]}{[\mathbf{Ia}]+[\mathbf{IIa}]} \quad (2)$$

Between ca. 2–14 grams of sediment (g_{sed}) were extracted for each sample, resulting in brGDGT concentrations ranging from 7 ng/g_{sed} to 1.58 µg/g_{sed}. Crenarchaeol concentrations ranged from 0.1 ng/g_{sed} to 0.8 µg/g_{sed}. Duplicates of 69 samples were run 5–8 months after the first injection with root mean square errors (RMSE) on BIT, MBT, and CBT measurements of 0.015, 0.007, and 0.041, respectively (Fig. 2). In addition 41 samples were run using a new method that improves the separation of brGDGTs (Hopmans et al., 2016). For samples run on both methods, the RMSEs were 0.08, 0.05, and 0.10 ($n = 41$) (Fig. 2). A complete comparison of the two methods is available in the supplementary materials.

3.3. *n*-alkane analysis

Plant leaf waxes (*n*-alkanes) form the waxy surface of terrestrial plant leaves, and can be short- (e.g. C_{17}–C_{21}, characteristic of aquatic organisms) or long-chained (C_{27}–C_{33}, characteristic of terrestrial higher plants) (Eglinton and Hamilton, 1967). For *n*-alkane analyses, apolar fractions were first injected on a Agilent 7890A dual gas chromatograph-flame ionization detector (GC-FID) with an Agilent 7693 autosampler equipped with a 5% phenyl methyl siloxane column (HP-5, 60 m × 0.32 mm × 0.25 µm). The oven program ramped from 70 °C to 130 °C at a rate of 10 °C min^{-1}, then from 130 °C to 320 °C at a rate of 4 °C min^{-1}, and held the final temperature for 10 min. Quantification was achieved by an external calibration curve of squalane ranging in concentration from 1 ng/µl to 100 ng/µl. The *n*-alkanes were identified by a Hewlett Packard 6890 gas chromatograph coupled to an Agilent 5973 Mass Selective Detector equipped with a 5% phenyl methyl siloxane column (HP-5MS, 60 m × 0.25 mm × 0.25 µm), with an identical oven program to the GC-FID. We calculate average chain length (ACL) using the fractional abundance ($f(C_n)$) of odd-carbon-number *n*-alkanes between C_{21} and C_{33} (Poynter and Eglinton, 1990).

$$ACL = \sum_{n=21}^{33} n \times f(C_n) \quad (3)$$

Samples with sufficiently high *n*-alkane concentrations for isotope analysis were separated into saturated and unsaturated fractions by elution over activated $AgNO_3$ columns with hexane (saturated fraction) and ethyl acetate (unsaturated fraction). δD_{wax} mea-

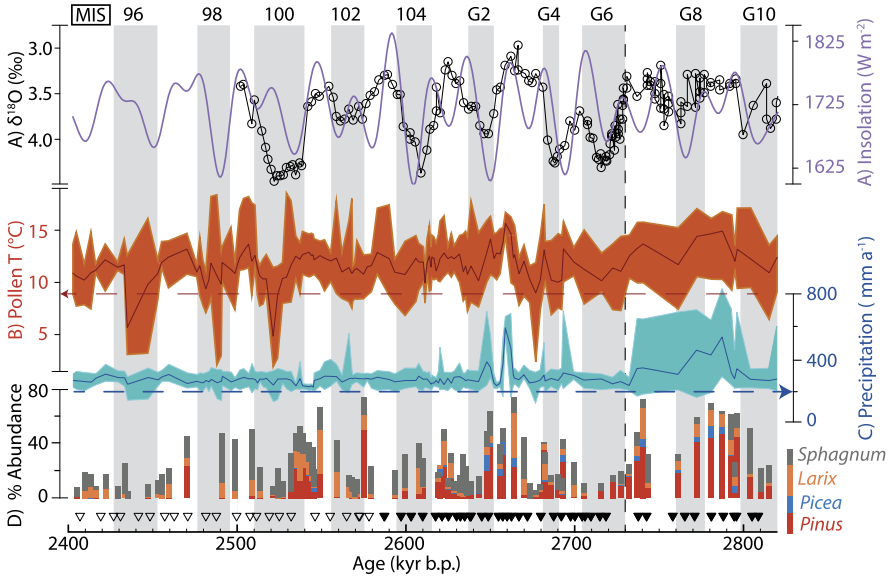

Fig. 3. Previously published temperature and hydrological reconstructions from Lake El'gygytgyn. MIS and age-model tie points (triangles) are as in Fig. 2. Colored envelopes give the absolute error for the reconstructions. A) The $\delta^{18}O$ record from ODP Site 1208 in the North Pacific (Woodard et al., 2014). Integrated summer (MJJA) insolation from Laskar et al. (2004) is plotted on the right-hand axis. B) Reconstructed mean temperature of the warmest month (MTWM) from pollen assemblages (Brigham-Grette et al., 2013). C) Reconstructed mean annual precipitation from pollen assemblages (Brigham-Grette et al., 2013). D) Percentage abundance of *Pinus*, *Picea*, *Larix* and *Sphagnum* pollen (Brigham-Grette et al., 2013).

surements were achieved on C_{29} *n*-alkanes by gas chromatography-isotope ratio monitoring mass spectrometry (GC-irMS). A Thermo Trace GC Ultra equipped with a 5% phenyl methyl siloxane column (HP-5, 60 m × 0.32 mm × 0.25 µm) was coupled to a reactor operated at 1450 °C, which was connected to a Thermo Delta V Advantage iRMS. The oven program held 70 °C for 2 min, ramped at 20 °C min^{-1} to 145 °C, then ramped at 4 °C min^{-1} to 320 °C and held for 13 min. Molecular deuterium/hydrogen ratios are reported in standard delta (‰) notation relative to the Vienna Standard Mean Ocean Water (VSMOW) and calculated following Polissar and D'Andrea (2014). All samples were run in duplicate or triplicate, bracketed by three injections of H_2 reference gas, with lab internal standards of known isotopic composition run between each sample and three times at the beginning and end of each instrument run to track inter-sample drift. A standard mixture containing C_{16}–C_{30} *n*-alkanes (Schimmelmann A5 standard) with known δD values ranging from -9 ± 1.4‰ to -254 ± 1.5‰ versus VSMOW was run upon reactor installation to determine the isotopic composition of the reference gas.

3.4. Time series analysis

To estimate the spectral characteristics of our reconstructions, we used the robust locally-weighted regression spectral background estimation (LOWSPEC) in the Astrochron R program (Meyers, 2012, 2014), which has high statistical power for correctly identifying frequencies in the obliquity and precession bands (Meyers, 2012, 2014). Briefly, the algorithm includes prewhitening, spectrum estimation using the multitaper method (Thomson, 1982), estimation of the spectral background and assignment of confidence levels using a Chi-square distribution. Using the LOWSPEC method, we identified the frequencies that satisfied a 95% LOWSPEC confidence level and a 95% multitaper method harmonic F-test confidence level (Meyers, 2012). All time series were analyzed by interpolating the data every 2.5 kyr from 2.41 to 2.82 Ma. For all LOWSPEC parameters, Astrochron default values were used (Meyers, 2014).

4. Results and discussion

In the following discussion, we make reference to the distinctive Lake El'gygytgyn sedimentary facies described in previous studies and the supplementary materials (Gebhardt et al., 2013; Brigham-Grette et al., 2013). The two facies of note are glacial facies A, a gray laminated facies thought to represent year-round lake ice cover, and super-interglacial facies C, a red laminated facies thought to represent extreme warmth and high autochthonous productivity (Gebhardt et al., 2013). We also compare our observations with previously published, pollen-based estimates of temperature and precipitation (Fig. 3) (Andreev et al., 2014). MIS definitions are from Lisiecki and Raymo (2005) and all data are on the original age model of Nowaczyk et al. (2013). We begin with a discussion of proxy interpretation and then examine notable features of the Lake El'gygytgyn record.

4.1. Proxy interpretation

There are several potential sources of brGDGTs to Lake El'gygytgyn sediments including the watershed soils/permafrost, inflowing streams, aeolian inputs, and in-situ water column production. Aeolian inputs are unlikely to be a major source of brGDGTs at Lake El'gygytgyn because they comprise less that 2% of the total sediment supply (Fedorov et al., 2013). Lake El'gygytgyn is surrounded by permafrost with a shallow active layer (<0.5 m) and brGDGTs are present in this material (Bischoff et al., 2014). However, watershed soils/permafrost are unlikely to comprise the main source of brGDGTs because snowmelt is the main yearly hydrological event and occurs when the ground is frozen, which limits erosion (Nolan and Brigham-Grette, 2007). Likewise, it is unlikely that the 50 small streams surrounding the lake represent the main brGDGT source as many are only active during the snowmelt period. Previous studies have noted that brGDGTs are abundant in Lake El'gygytgyn sediments and that the MBT/CBT palaeothermometer is sensitive to temperature changes on glacial–interglacial timescales there (D'Anjou et al., 2013; de Wet et al., 2016; Holland et al., 2013). Given ample evidence for *in situ* production of brGDGTs at other lakes, either within the water col-

umn or in the sediments themselves (e.g. Buckles et al., 2014; Loomis et al., 2014), we assume that brGDGTs are produced within the Lake El'gygytgyn water column. A main source of brGDGTs from within the sediments seems improbable as bottom water temperatures exhibit little variability (3–4 °C between winter and summer) (Nolan and Brigham-Grette, 2007) and in such a large, deep lake are unlikely to change much even on glacial–interglacial timescales. Thus, we assume that brGDGTs are produced in the lake surface waters and surmise that they likely reflect mean summer temperature (MST (°C)) given that at Lake El'gygytgyn, ice-cover for 10 months of the year restricts most primary production to July and August. Similarly, Shanahan et al. (2013b) found that MBT/CBT-derived temperatures inferred from lake sediments across Baffin Island reflected mean summer temperatures while several other studies have suggested summer brGDGT production (e.g. Schoon et al., 2013; Foster et al., 2016).

In addition to the aforementioned global soils calibrations (Weijers et al., 2007b; Peterse et al., 2012), numerous lacustrine brGDGT calibrations from different environments have been proposed (e.g. Tierney et al., 2010; Loomis et al., 2012; Foster et al., 2016). For this study, we choose to apply the calibration of Sun et al. (2011) for lakes with pH < 8.5.

$$MAAT\ (^{\circ}\mathrm{C}) = 3.949 - 5.593 \times CBT + 38.213 \times MBT \quad (4)$$

Sun et al. (2011) studied lakes on the arid Tibetan Plateau, representing some of the geographically closest samples to Lake El'gygytgyn analyzed for brGDGTs. In support of our assumptions, reconstructed MST from Holocene sediments using this calibration (6.5 °C) (Holland et al., 2013) are within calibration error of pollen-based mean temperature of the warmest month (MTWM) estimates (10 °C) and observed summer temperatures (9 °C) (Brigham-Grette et al., 2013). However, we note that applying different lacustrine brGDGT calibrations also yields Holocene temperatures in general agreement with the pollen based estimates. For this reason, we recommend considering the MBT/CBT data presented here as a relative temperature indicator because overall trends observed (e.g. warmings and coolings) are unaffected by the choice of calibration. Therefore, we interpret the MBT/CBT record as an *in situ*-produced signal reflecting mean summer temperature at Lake El'gygytgyn.

Long-chain *n*-alkanes with odd-over-even chain-length predominance are characteristic of terrestrial higher plants. At some locations ACL is positively correlated to temperature (e.g. Bush and McInerney, 2015) but increased aridity can also result in higher ACL values (e.g., Andersson et al., 2011). Although ACL has not been investigated in Arctic lakes, we expect ACL to share variance with pollen-based reconstructions of temperature or precipitation from Lake El'gygytgyn, since the *n*-alkanes and pollen likely have a similar source. Short-chain *n*-alkanes can be produced by aquatic organisms, and thus changes in ACL could be driven by an aquatic rather than terrestrial signal. However, some of the local vegetation around Lake El'gygytgyn produces high concentrations of C_{20}–C_{24} *n*-alkanoic acids suggesting the shorter *n*-alkanes may be terrestrially derived as well (Wilkie et al., 2013). Therefore, we interpret changes in ACL as reflecting changes in terrestrial vegetation.

The deuterium to hydrogen ratio (δD) of plant leaf waxes reflects the δD of precipitation (δD_P), which depends on the extent of Rayleigh distillation of a precipitating water mass (Dansgaard, 1964). At high latitudes, modern δD_P is strongly correlated with MAAT (°C). However, other factors contribute to the final δD_{wax} signal. Changes in δD_{wax} may also reflect changes in local vegetation via changes in mean biosynthetic fractionation, because, for example, woody gymnosperms fractionate less strongly than grasses during alkane synthesis (Sachse et al., 2012). Previously published pollen records from Lake El'gygytgyn provide an independent means of assessing when vegetation turn-over may influence the δD_{wax} reconstructions. Moisture sources and trajectories also exert a secondary effect on δD_P, which would be entrained in the δD_{wax} signal (Dansgaard, 1964), although there is currently no independent method for assessing this. Additional details about the numerous controls on this proxy are available in the supplementary materials. However, because of the strong coherence between instrumental temperatures, MBT/CBT temperatures, and δD_P in the modern Arctic (Shanahan et al., 2013b; Shanahan et al., 2013a), we expect MBT/CBT and δD_{wax} to share a majority of their variance on glacial–interglacial timescales. We interpret divergence of the MBT/CBT and δD_{wax} as reflecting a change in proxy systematics, with the dominant control on one or both of the proxies differing in the palaeo-setting from what it is today. The most likely factors to have influenced either of these proxies are changes in vegetation, insolation, seasonality, ocean temperatures, sea level, and the extent of both sea and land ice, all of which were considerably different during the Pliocene. In the forthcoming sections, we discuss the coherence of the newly presented proxy records (MBT/CBT and δD_{wax}) in the context of known variations of these other factors. We find that δD_{wax} does not covary with our MBT/CBT temperature reconstruction or previously published pollen-based temperature reconstructions, suggesting shifting moisture sources were an important control on Pliocene δD_{wax} values.

4.2. Main features noted during MIS G10–95

To facilitate comparison between different glacial and interglacial periods, below we report mean values for MBT/CBT temperatures when applying the Sun et al. (2011) calibration. However, we wish to emphasize that the values reported here are calibration dependent and absolute temperatures should be interpreted with caution.

4.2.1. MIS G10–G4

MIS G10–G4 show glacial–interglacial variability in the MBT/CBT and pollen records (Fig. 4D). MBT/CBT temperatures range from 5.5 °C (G6) to 11 °C (G7). For MBT/CBT, mean glacial (interglacial) temperatures are 8.2 °C (8.7 °C), and for pollen they are 11.8 °C (12.8 °C). Temperature reconstructions accord with physical sediment changes, with facies C occurring during the warm periods MIS G9 and G7. The δD_{wax} record documents broadly stable values between −265‰ and −275‰ until MIS G4. δD_{wax} values decrease from −265‰ to −275‰ over ∼10 kyr during the transition from MIS G7 to MIS G6 (Fig. 4C). Variability within MIS stages is greater in the MBT/CBT and pollen records compared with the stable δD_{wax} values during this period (Fig. 3B, Fig. 4C, D). The mean ACL value for MIS G10–G4 is 28.5, with slightly higher ACL during MIS G10 and G6 and slightly lower ACL during G8 and G7. Changes in ACL generally track changes in MBT/CBT during this period (Fig. 4B, D).

4.2.2. MIS G3–101

From MIS G3–101, intra-MIS variability is greater than inter-MIS variability. As a result, changes in mean values between glacial and interglacial periods are small (Fig. 4D). The most extreme glacial (interglacial) values in the MBT/CBT record reach 5 °C (14 °C), an increased range compared to MIS G10–G4. For MBT/CBT, mean glacial (interglacial) temperatures are 9.2 °C (9.5 °C), and for pollen they are 11.8 °C (12.1 °C). The two records show many similar features, including pronounced warmth during MIS G3 and mild glacial conditions during MIS 104 (Fig. 4D, Fig. 3B). The first appearance of glacial facies A at MIS 104 contrasts with the modest cooling observed in the temperature reconstructions, and multiple excursions to similarly low temperatures during other glacial stages (e.g. MIS 100) do not feature facies A. After a period of rapid

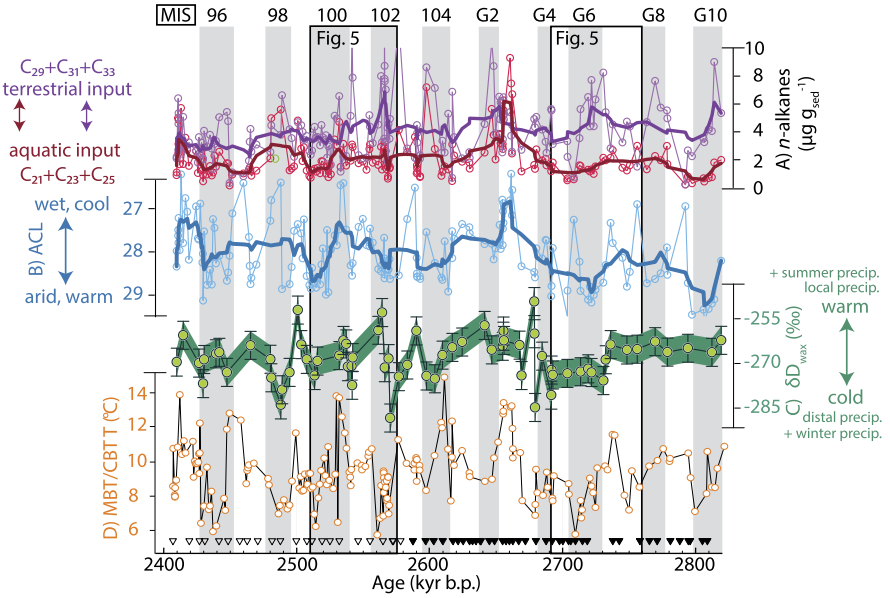

Fig. 4. New temperature and hydrological reconstructions from Lake El'gygytgyn. MIS and age-model tie points (triangles) are as in Fig. 2. A) Total *n*-alkane concentrations. In purple, the sum of all C_{27} to C_{33} *n*-alkanes. In red, the sum of all C_{21} to C_{25} *n*-alkanes. All data points are shown in the background and the thick lines represent a 7-point (~10 kyr) running mean. B) Average chain length (ACL) of C_{21} to C_{33} *n*-alkanes, with high values indicating warm or arid conditions, and low values indicating cool or dry conditions. C) δD_{wax} on the VSMOW scale, calculated following Polissar and D'Andrea (2014). D) Reconstructed temperatures from MBT/CBT using the calibration of Sun et al. (2011).

isotopic enrichment during MIS G3, the δD_{wax} record shows positive trend culminating in a mean value of −261‰ during MIS G2, followed by a negative trend to a minimum mean of −272‰ during MIS 104 and, after an increase to −260‰ during MIS 103, falls to −290‰ during MIS 102 (Fig. 4C). MIS 102 is differentiated by cool but especially variable MBT/CBT temperatures (Fig. 5F). The mean ACL value for MIS G3–101 is 27.8. The lowest ACL values in the record occur during MIS G3. As in MIS G10–G4, changes in ACL track changes in MBT/CBT (Fig. 4B, D).

MIS G3 is the warmest interval of both pollen- and brGDGT-based temperature reconstructions. Initially we found an unknown compound co-eluting with brGDGT **Ib** in the 15 kyr interval spanning 2.651 to 2.665 Ma that led to unrealistically high reconstructed temperatures (>30 °C). However, when re-analyzed using a newer method that dramatically improves chromatographic separation of brGDGT isomers (Hopmans et al., 2016), the formerly co-eluting compound was completely separated, yielding maximum temperatures of <15 °C. MIS G3 is marked by a large increase in the amount of *Picea* pollen (Fig. 3D), high reconstructed precipitation, and ^{2}H-enriched δD_{wax} (−260‰), suggesting a short-lived, but perhaps dramatic, climatic change.

4.2.3. MIS 100–95

MIS 100–95 show the most pronounced change between glacial and interglacial periods of any part of the MBT/CBT and δD_{wax} records. MBT/CBT temperatures range from 5 to 14 °C, similar to MIS G3–101, but the mean changes now show coherence on glacial–interglacial timescales, in contrast to MIS G3–101. For MBT/CBT, mean glacial (interglacial) temperatures are 8.2 °C (9.1 °C), and for pollen they are 10.2 °C (11.9 °C). Mean glacial (interglacial) δD_{wax} values are −271‰ (−264‰). In addition, δD_{wax} and MBT/CBT-derived temperature are strongly correlated from MIS 100–98 (2446–2518 kyr, $r = 0.76$, $n = 12$, $p = 0.01$, see supplementary materials). Nevertheless, the MBT/CBT and δD_{wax} records each show unique features during this interval. A 4 °C cooling in the MBT/CBT record during MIS 100 (ca. 2520 kyr) is not expressed in the δD_{wax} record (Fig. 5E, F). In addition, ^{2}H-depleted *n*-alkanes are observed during MIS 98 in the absence of cooling in the MBT/CBT record (Fig. 4C, D). Laminated glacial facies A appears

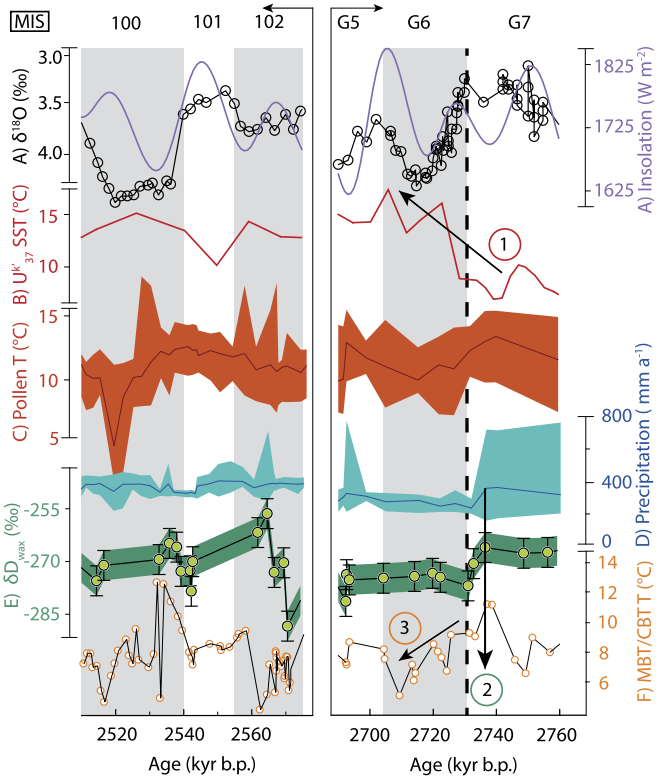

Fig. 5. Detail view of MIS 100–102 and G5–G7. A) The benthic $\delta^{18}O$ record from ODP Site 1208 in the North Pacific (Woodard et al., 2014). Integrated summer (MJJA) insolation from Laskar et al. (2004) is plotted on the right-hand axis. B) Alkenone-based SST reconstruction from ODP Site 882 (Martínez-Garcia et al., 2010). C) Reconstructed mean temperature of the warmest month (MTWM) from pollen assemblages (Brigham-Grette et al., 2013). D) Reconstructed mean annual precipitation from pollen assemblages (Brigham-Grette et al., 2013). E) δD_{wax} on the VSMOW scale, calculated following Polissar and D'Andrea (2014). F) Reconstructed temperatures from MBT/CBT using the calibration of Sun et al. (2011). Numbers annotate features discussed in the text: 1) North Pacific warming at iNHG, 2) crash in precipitation and depletion of δD_{wax} at iNHG, 3) gradual cooling at Lake El'gygytgyn following iNHG.

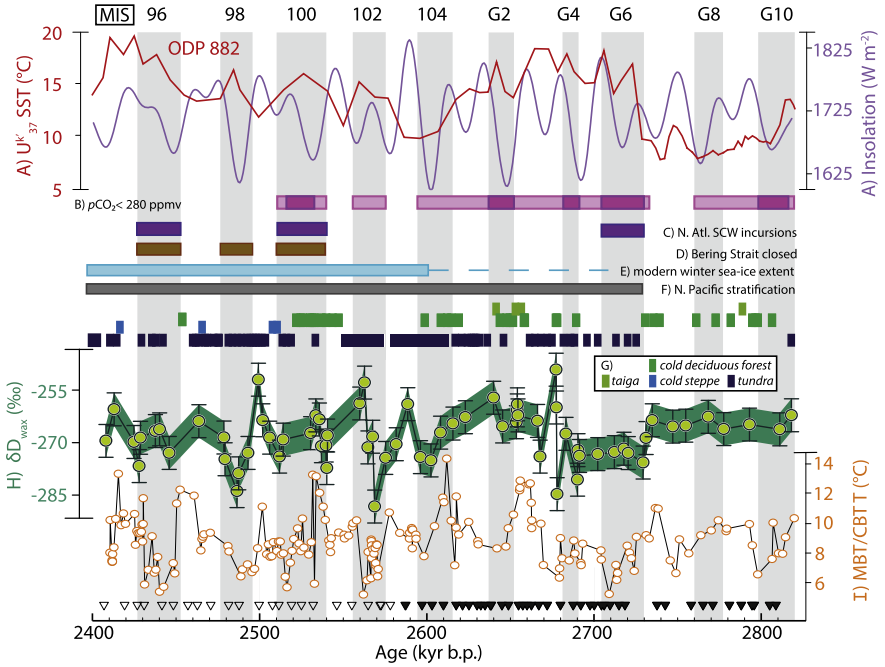

Fig. 6. Summary of Arctic palaeoenvironmental reconstructions. MIS and age-model tie points (triangles) are as in Fig. 2. A) Alkenone-based SST reconstruction from ODP Site 882 (Martínez-Garcia et al., 2010). Integrated summer (MJJA) insolation (Laskar et al., 2004) is plotted on the right-hand axis. B) In pink, times reconstructed pCO_2 from Martínez-Botí et al. (2015) falls below the threshold for Northern Hemisphere glaciation (in light pink, within one sigma) (DeConto et al., 2008). C) In purple, periods where southern component water bathed the North Atlantic (Lang et al., 2016). D) In brown, times of Bering Strait closure estimated from the global sea-level record of Miller et al. (2012). E) In blue, onset of sea-ice from Knies et al. (2014). F) In gray, onset of North Pacific stratification inferred by Haug et al. (2005). G) Below, pollen based biome reconstructions from Lake El'gygytgyn (Brigham-Grette et al., 2013) are as follows: taiga (light green), cold deciduous forest (dark green), cold steppe (blue), tundra (indigo). H) Lake El'gygytgyn δD_{wax}. I) Lake El'gygytgyn MBT/CBT temperature.

during MIS 98 and 96, two of the coldest and most ^{2}H-depleted parts of the reconstruction (Fig. 4C, D). The mean ACL value during this period is 27.8. Higher ACL values (29) occur during MIS 100, and lower ACL values (27.1) occur during MIS 95 (Fig. 4B).

4.3. Proxy coupling and time series analysis

Interestingly, MBT/CBT temperatures and δD_{wax} are decoupled for most of the record. The only period when they share significant variation is MIS 100–96 (Fig. 4C, D). In addition, both proxies show an increase in range following MIS G6. The range of the MBT/CBT record increases from 5.5 to 11 °C before MIS G6 to 5 to 14 °C afterwards (Fig. 4D). δD_{wax} also shows an increase in range, from −275 to −265‰ before MIS G6 to −290 to −240‰ afterwards (Fig. 4C). Nevertheless, the distinct behavior of the MBT/CBT and δD_{wax} proxies, which we expect to be highly correlated, suggests one or both are recording changes in environmental parameters other than temperature. The pollen and MBT/CBT records generally show similar features and are positively correlated for the duration of our study ($r = 0.5$, $n = 182$, $p = 0.01$). Thus we conclude that the MBT/CBT record is a good representation of past temperature, as expected. In contrast, the δD_{wax} record shares very little variation with the pollen and MBT/CBT records, suggesting temperature was not the dominant control on this proxy for most of the interval studied. Instead, changes in moisture source likely exerted an important control on the δD_{wax} record in addition to temperature.

To further interrogate the distinct proxy responses across the study interval, we looked at the spectral characteristics of each of these signals. First, we analyzed the benthic δ^{18}O stack (Lisiecki and Raymo, 2005) and integrated summer insolation (Laskar et al., 2004). The dominant frequencies identified by LOWSPEC were 40 kyr for the benthic δ^{18}O stack and 40, 29, 22, 18, 16 and 11 kyr for the integrated summer insolation (Fig. 7A, B, C). Next, we performed the same analysis on our time series. The dominant frequencies identified for our proxy records were: 39 kyr for MBT/CBT (Fig. 7D); 39.6 kyr for the pollen-based temperature reconstruction (Fig. 7E); 25, 15, and 5 kyr for the ACL record (Fig. 7F); and 30 kyr for the δD_{wax} record (Fig. 7G). From this analysis, it is apparent that the brGDGTs and pollen are both responding to obliquity-band forcings (i.e. glacial–interglacial cycles) shared with the benthic δ^{18}O stack. In contrast, the *n*-alkane records, ACL and δD_{wax}, vary in response to precession-band forcings shared with the integrated summer insolation (Laskar et al., 2004) (Fig. 7H). This result confirms that temperature variability in Siberia was partially decoupled from hydrological and vegetation changes during the Late Pliocene. In the following sections, the potential influences of vegetation, pCO_2, insolation, seasonality, changes in oceanography, sea ice, and land ice on the new MBT/CBT and δD_{wax} records are discussed.

4.3.1. Influence of vegetation change on the n-alkane records

ACL varies out-of-phase with MBT/CBT reconstructed temperature, with low ACL values during warm interglacial periods ($r = -0.34$ with 5-point smooth, $n = 164$, $p < 0.01$) (Fig. 4B). This suggests that ACL may be partially controlled by temperature at Lake El'gygytgyn. If *n*-alkane distributions are also controlled by aridity at Lake El'gygytgyn, we expect to see a correspondence between ACL and reconstructed precipitation. Indeed, the most pronounced precipitation peak inferred from the pollen record corresponds to the lowest ACL values (MIS G3, Fig. 3C, Fig. 4B). However, during the earliest part of the record (MIS G10–G7), when pollen assemblages suggest high reconstructed precipitation, ACL values are also high. The stepped transition from a forest- to tundra-dominated landscape during this period undoubtedly complicates the use of ACL as an aridity proxy (Brigham-Grette et al., 2013). However, large fluctuations in ACL occur after tundra became firmly established during MIS 102 (Fig. 6G). It is possible that our

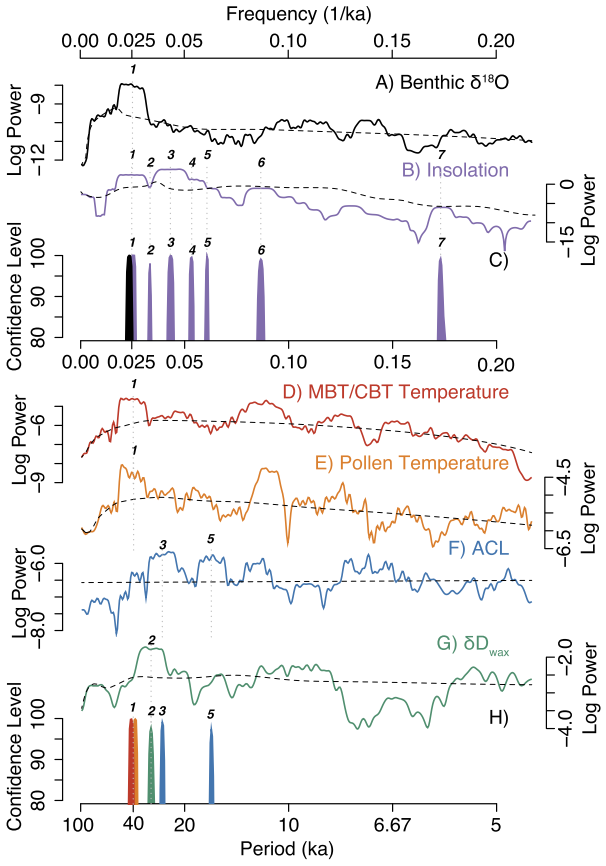

Fig. 7. Spectral characteristics of global climate records and Lake El'gygytgyn proxy records. Black dotted lines indicate the LOWSPEC background (Meyers, 2014). Peaks in C) and H) are only shown if they satisfy both the LOWSPEC and MTM harmonic F-test 95% confidence levels. A) The benthic $\delta^{18}O$ stack (Lisiecki and Raymo, 2005). B) Integrated summer (MJJA) insolation (Laskar et al., 2004). C) Spectral peaks reaching the 95% confidence level for panels A and B. D) MBT/CBT temperature (this study). E) Pollen temperature (Brigham-Grette et al., 2013). F) *n*-alkane average chain length (ACL, this study). G) δD_{wax}. H) Spectral peaks reaching the 95% confidence level for panels D–G.

n-alkane record reflects climatically-driven changes in plant community composition that are not captured by the lower-resolution pollen record (Fig. 3D). Such fluctuations would serve as a positive feedback to climatic change via changes in albedo, although the length of this record is not adequate to address whether such a mechanism was firmly developed by the Early Pleistocene.

Changes in δD_{wax} may also reflect changes in local vegetation via changes in mean biosynthetic fractionation. If this were the dominant control, we would expect to see changes in biosynthetic fractionation due to the advance and retreat of the treeline, which represents a substantial change to the dominant biome and thus, the source of *n*-alkanes. However, the δD_{wax} record does not track large changes in tree-cover (i.e. the return of *Picea* during MIS G3, Fig. 3D) supporting that the δD_{wax} record mainly reflects δD_P rather than tracking changes in biosynthetic fractionation.

4.3.2. pCO_2, insolation and seasonality

Reconstructed pCO_2 through the Plio-Pleistocene transition lacks the resolution to assess the change in pCO_2 forcing for each glacial and interglacial stage represented in the current study, but there are some similarities of note (Martínez-Botí et al., 2015). The largest excursion in the pCO_2 record occurs across iNHG, with pCO_2 dropping from ~350 ppm at MIS G7 to ~250 ppm at MIS G6, an interval across which we observe a MBT/CBT cooling and a change from stable to variable δD_{wax} (Fig. 6B, H, I). The resolution of the pCO_2 record is inadequate to assess the amplitude of pCO_2 forcing for MIS 95–99, which are large amplitude glacial–interglacial cycles in our record and most coherent between proxies (Fig. 6H, I). However, future work should take advantage of the high-resolution records we provide here to assess Arctic climate sensitivity to pCO_2 during the Pliocene.

Although integrated summer insolation at 65°N is an important forcing of high-latitude climate change, the MBT/CBT record does not show a strong influence of insolation (Huybers, 2006). From MIS 95–99, we observe large fluctuations in MBT/CBT even though the changes in insolation are small (Fig. 6A, I). During MIS G3, peaks in MBT/CBT temperature and δD_{wax} are offset from one another, but align with distinct peaks in summer insolation (Fig. 6A, H, I). Our time series analysis shows that the MBT/CBT and pollen records vary on 40 kyr timescales, in line with the importance of obliquity forcing at high latitudes (Huybers, 2006). In contrast, the ACL and δD_{wax} records also contain significant power at higher frequencies within the precession band (25–19 kyr).

Throughout the record changes in reconstructed temperature and δD_{wax} are decoupled, with higher temperatures occurring during periods of ^{2}H-depleted precipitation (and vice-versa). Changes in seasonality might explain some of this behavior. Indeed, Hennissen et al. (2015) found that seasonality in the North Atlantic increased following MIS G3, caused by a decrease in spring temperatures that was especially pronounced during glacial periods. If this led to a decrease in winter precipitation and an increase in summer precipitation at Lake El'gygytgyn, we would expect higher δD_{wax} values even during glacial periods, which we see in parts of our record (i.e. MIS G2, 104, 102 in Fig. 4D). We also reconstruct only modest cooling during MIS 104, a glacial period with heavy ice rafting in the North Atlantic and Nordic Seas, which may suggest an imprint of seasonality on the MBT/CBT record as well (Kleiven et al., 2002). Hennissen et al. (2015) suggest that the change in seasonality was a threshold effect resulting from dynamical consequences of growing Northern Hemisphere ice volume. We find that the coherence between MBT/CBT and δD_{wax} varies between adjacent glacial periods, which could be related to changes in seasonality. For example, some glacial periods feature ^{2}H-enriched precipitation despite much lower temperatures (MIS 96, Fig. 4D, E) but other glacial periods show both ^{2}H-depleted precipitation and reduced temperature (MIS 98, Fig. 4D, E). Our data, in combination with marine records, lends credence to recent modeling work that demonstrated seasonality during the Pliocene depends on the precise orbital configuration of the earth (e.g. Prescott et al., 2014).

4.3.3. Sea ice and oceanic influences

Haug et al. (2005) show that stratification and seasonal warming occurred in the North Pacific around 2.73 Ma (MIS G6), which would lead to increased annual precipitation and more ^{2}H-enriched precipitation in the Arctic. In contrast, pollen-based biome reconstructions at Lake El'gygytgyn suggest a dramatic decrease in mean annual precipitation at 2.73 Ma (MIS G6) (Brigham-Grette et al., 2013), when δD_{wax} becomes more ^{2}H-depleted. Thus, the environmental changes at Lake El'gygytgyn during iNHG contradict what we expect to see.

Another component of the high-latitude climate system that underwent a dramatic transition around MIS G6 is sea ice. Unfortunately, Arctic sea-ice records across the Plio-Pleistocene lack the resolution to assess changes on glacial–interglacial timescales pertinent to this study. According to one study, around MIS 100 sea-ice extent similar to the present day was possible (Knies et al., 2014). In addition, the outlet of the Yukon river shifted from the North Pacific to the Bering Sea coincident with the first glaciation of the Canadian Arctic around MIS 104 (Duk-Rodkin and Hughes, 1994). This new source of freshwater would have catalyzed production of sea-ice, which intensified during iNHG in the Bering Sea

(Takahashi et al., 2011). If an ice-free Arctic Ocean was a source of precipitable moisture to Siberia during the Pliocene, sea-ice advance would cause reduced mean annual precipitation and more ^{2}H-depleted δD_P (via increased Raleigh distillation). This is exactly the combination of changes we observe from pollen and δD_{wax} during MIS G6 (Fig. 5D, E). However, the paucity of sea-ice and SST records from the Pliocene Arctic make this mechanism difficult to directly test.

Recent modeling work indicates it is not clear what the net effect of increased sea-ice cover on δD_P at Lake El'gygytgyn would be. The isolation of the Arctic Ocean and higher precipitation rates during the Pliocene would have resulted in a $>10‰$ isotopic depletion of Arctic surface waters (Tindall and Haywood, 2015). Thus, we might expect a decrease in Arctic-sourced precipitation to result in isotopic enrichment of δD_P, which would counter the isotopic effect of increased Raleigh distillation over the sea-ice. Our work demonstrates that the effects of sea-ice expansion from a Pliocene background climate state should be explored further.

Changes in surface ocean conditions also affect continental interior temperatures. Haug et al. (2005) hypothesized that seasonal warming of the North Pacific resulted in greater moisture availability for high northern latitudes. Sea surface temperatures in the North Pacific (Martínez-Garcia et al., 2010) begin to warm during MIS G7, culminating in a period of prolonged higher temperatures from MIS G6–G2. In contrast, the pollen record from Lake El'gygytgyn suggests a severe drop in precipitation at MIS G6, from Pliocene values of 800 mm a^{-1} to near-modern values of 200 mm a^{-1}, and the MBT/CBT record shows a gradual cooling through MIS G7–G6 (Fig. 5E, F). Thus, the evidence from Lake El'gygytgyn is inconsistent with increased advection of latent and/or sensible heat from the North Pacific following iNHG. On the other hand, previous studies have shown the important role that an open Arctic Ocean can play in warming continental interiors via the transport of latent and sensible heat (Ballantyne et al., 2013). A reduction in heat and moisture transport to Lake El'gygytgyn following the establishment of sea-ice during MIS G7/G6 is a more consistent mechanism for producing the changes we observe. Ballantyne et al. (2013) also found that the net radiative effect of sea-ice is to dramatically increase the annual range of temperatures. The increased amplitude temperature variations we reconstruct following MIS G6 suggests that this radiative effect may also have been important on glacial–interglacial timescales during the Late Pliocene.

4.3.4. Ice sheets, sea level and the Bering strait

Prior to iNHG, it is assumed that most of the global eustatic sea-level variations were driven by changes in Antarctic ice volume. During iNHG, the pace of Northern Hemisphere glaciation accelerated rapidly and a semi-permanent ice-sheet was established on Greenland (DeConto et al., 2008). While earlier glaciations occurred in the Northern Hemisphere at least as early as the middle Pliocene, data suggests that North America certainly hosted a mature, marine-terminating continental ice sheet, beginning at ~2.64 Ma (MIS G2) (DeSchepper et al., 2014; Bailey et al., 2013). However, Late Pliocene/Early Pleistocene ice sheets were especially unstable. Funder et al. (2004) describe a Late Pliocene terrestrial sequence (Member A of the Kap København formation, ca. ~2.5–2.4 Ma, MIS 98–95) from Northeast Greenland that implies a 40 m marine transgression and summer warming in excess of 15 °C (Fig. 1). These data suggest near-complete deglaciation of the Northern Hemisphere and the return of Pliocene-like conditions to the circum-Arctic after an early Pleistocene glaciation. Indeed, Brigham-Grette and Carter (1992) describe three marine transgressions of Late Pliocene/Early Pleistocene age from Alaska. The earliest two of these (the Colvillian and Bigbendian transgressions) contain *Pinus* and *Picea* pollen, while the final (Fishcreekian) contains mostly tundra pollen with some *Larix*. It is tempting to link the Kap København formation and Colvillian transgression with the pronounced MIS G3 warmth at Lake El'gygytgyn, as all are coeval within age model uncertainty. However, large age model uncertainties in the discontinuous records preclude precise correlations at this time. The Bigbendian transgression contains the Matuyama-Gauss magnetic reversal (MIS 103) and is therefore unequivocally represented in our study period. Our reconstructions do not show notably high temperatures or ^{2}H-enriched precipitation during this interval, both of which we might expect to see during a sea level transgression up to +40 m. Regional records also show unremarkable changes during MIS 103: benthic δ^{18}O and alkenone SSTs from the North Pacific depict a mild interglacial climate (Woodard et al., 2014; Martínez-Garcia et al., 2010).

It is also uncertain how changes in sea level would affect our reconstructions. Due to the shallow bathymetry of the Bering Strait, changes in sea level can result in a dramatic increase in continentality for interior Beringia (Fig. 8C, D). New reconstructions of Pliocene palaeogeography argue for a closed Bering Strait ~3 Ma, with global eustatic sea level more than 20 m above present, suggesting that the region has seen significant erosional or tectonic subsidence since that time (Dowsett et al., 2016). However, observations of Pliocene shorelines on the Diomede Islands attest to hundreds of meters of regional uplift in the last few million years, which is difficult to reconcile with a subaerial Bering Strait during the Pliocene (Gualtieri and Brigham-Grette, 2001). We find an increase in the glacial–interglacial range of MBT/CBT temperatures and δD_{wax} following iNHG. While decreasing glacial temperatures are consistent with regional albedo changes from the establishment of land-based ice sheets during glacial stages, increasing interglacial temperatures are more perplexing. As closure of the Bering Strait can enhance the Atlantic meridional overturning circulation and heat transport into the Arctic Basin (Hu et al., 2015), this may have been a mechanism for increased interglacial warmth following the increasingly severe glaciations after iNHG. If, as sea level records would indicate (Miller et al., 2012), the first closures of the Bering Strait occurred after MIS G6, this mechanism is plausible (Fig. 6D). However, this would also suggest that, at least for the earliest part of our record (2.82–2.73 Ma, MIS G10–G7), the Bering Strait remained open.

Our MBT/CBT and δD_{wax} reconstructions underscore the complex ways that expanding ice sheets drove, and responded to, Late Pliocene environmental change. For example, MBT/CBT reconstructions for MIS 102 indicate a very cold and variable glacial stage, corroborated by low δD_{wax} values, but global and regional benthic oxygen isotope records show a negligible change in global ice volume during this time (Fig. 5A, E, F) (Lisiecki and Raymo, 2005; Woodard et al., 2014). These results are consistent with the response we would expect to see from ice-sheet advance in Eastern Chukotka influencing both regional albedo and moisture pathways without affecting a significant change in bottom water oxygen isotopes (Niessen et al., 2013). The high percentage of *Larix* pollen (which is not subject to eolian transport, Andreev et al., 2014) during MIS G2, 104 and 100 suggests that these glacials were not particularly cold and/or the treeline persisted at 67.5°N in the Siberian Arctic despite glacial advances in other parts of the Northern Hemisphere. In contrast, MIS 98 and 96 contain little tree pollen, low reconstructed MBT/CBT temperatures, and ^{2}H-depleted δD_{wax}. The diversity of proxy responses between adjacent glacial stages speaks to the range of mechanisms that can drive glacial–interglacial climate changes in the terrestrial Arctic. Future modeling studies to explore the impact of ice-sheet advance in different regions of the Arctic could leverage the records presented here for deciphering the evolution of Northern Hemisphere vegetation and ice cover during the late Pliocene and early Pleistocene.

The increasingly variability of δD_{wax} during MIS G5 coincides with the increased delivery of *n*-alkanes to the North Atlantic

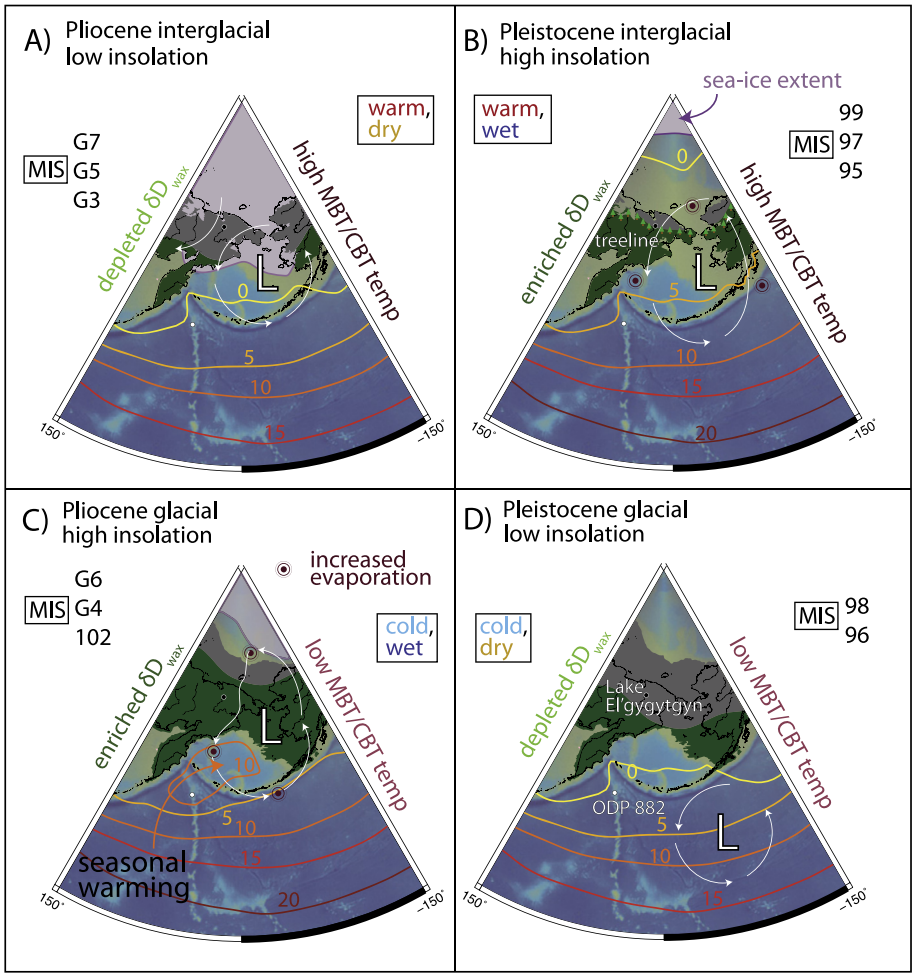

Fig. 8. Schematic depiction of environmental change in Beringia that could produce the observed proxy behavior. Panels A) and C) indicate idealized Pliocene-age "transition" scenarios, whereas B) and D) indicate conditions similar to those inferred for the Pleistocene. In all panels, background colors are bathymetry, gray shading indicates subaerial land area, black line indicates modern coastline, green shading indicates the treeline, arrows indicate idealized atmospheric circulation around the Aleutian Low ("L"), colored contours indicate sea surface temperature (°C), and white shading indicates sea-ice extent. All depictions are meant to be representative of mean annual conditions. The treeline contours are meant to be illustrative and do not represent real data. The sea surface temperature and sea ice contours are idealizations based on manual modification of satellite data (http://neo.sci.gsfc.nasa.gov). The black dot indicates the position of Lake El'gygytgyn. The white dot indicates the location of ODP Site 882 (Martínez-Garcia et al., 2010). Interglacial panels A) and B) are depicted with sea level +40 m above present. Glacial panels are depicted with sea level −125 m below present. A) Pliocene interglacial with low insolation. An advanced sea ice edge, southerly treeline, and reduced SSTs are depicted. B) Pleistocene interglacial with high insolation. A retreated sea ice edge, northerly advance of the treeline, and increased SSTs are depicted. Black dots highlight areas where additional moisture might enter the atmosphere. This scenario represents an extreme high sea-level interglacial, similar to those inferred in the Early Pleistocene. C) Pliocene glacial climate with high insolation. A retreated sea ice edge, northerly advance of the treeline, and elevated SSTs are depicted. A local maximum in SSTs is depicted in the North Pacific extending into the Bering Sea, meant to represent the seasonal warming and stratification hypothesized by Haug et al. (2005). Black dots highlight areas where additional moisture might enter the atmosphere. D) Pleistocene glacial climate with low insolation. An advanced sea ice edge, southerly treeline, and reduced SSTs are depicted, consistent with what is generally inferred for the Last Glacial Maximum.

(Naafs et al., 2012), which is attributed to increasing glaciogenic dust sources following iNHG. Notably, we observe a slight increase in the concentration of *n*-alkanes at Lake El'gygytgyn beginning with MIS G3, suggesting that an increased production of long-chain *n*-alkanes may be partially responsible for these observations. However, *n*-alkane concentrations in the North Atlantic clearly peak during glacial stages. Although *n*-alkane concentrations vary at Lake El'gygytgynm we do not observe any measurable difference between mean glacial and interglacial values (Fig. 4A). This reinforces the interpretation that increased *n*-alkane deposition during glacial periods in the North Atlantic is a result of greater erosion by ice-sheets, not increased terrestrial *n*-alkane production (Naafs et al., 2012). δD_{wax} and MBT/CBT show pronounced changes during MIS 102, one glacial stage prior to increased delivery of ice-rafted debris to the North Atlantic (Shackleton et al., 1984). Similar to findings from the marine realm of continued glacial intensification following MIS 100, our records show pronounced and coherent glacial–interglacial variability from MIS 100–95 (Fig. 4D, E) (e.g. Shackleton et al., 1984; Naafs et al., 2012; Kleiven et al., 2002).

4.4. The Lake El'gygytgyn record in global context

The MBT/CBT and δD_{wax} records presented here represent a continuous record of Arctic climate evolution. These reconstructions have implications for understanding independent components of the Arctic climate system, including the carbon cycle, sea ice extent, and continental ice sheet development. Importantly, they allow us to begin placing discontinuous and time-uncertain terrestrial records into perspective. Interpreting temperature and hydrological change in the early Pliocene Arctic is difficult because of the scarcity of records, but the hypotheses laid out here can be more rigorously examined as new records are developed for comparison.

Importantly, we document numerous stages when warm and dry, or cool and wet, conditions dominated at Lake El'gygytgyn during the Pliocene–Pleistocene transition. Due to the wide range of processes and mechanisms that could affect our reconstructions, there are multiple scenarios consistent with the MBT/CBT and δD_{wax} records (Fig. 8). Based on the results of our reconstructions and time series analysis, we find that vegetation (ACL) and moisture source (δD_{wax}) changes respond to changes in insolation. In our conceptual model of climate evolution during this interval, this corresponds to changes in the latitude of the treeline, the sea-ice edge, and North Pacific sea surface temperatures. In contrast, the MBT/CBT record follows glacial–interglacial variability in global climate and sea level. For Pleistocene interglacial and glacial periods, it is assumed that all of these factors vary, for the most part, synchronously (Fig. 8B, D)). For most of our record, the data indicate an alternative configuration was possible at Lake El'gygytgyn (Fig. 8A, C).

We suggest the following sequence of environmental changes best agrees with the multiple proxy records presented here. Stable warm conditions persisted from MIS G10–G7 in the Siberian Arctic, with at least seasonally ice-free conditions in the Bering and Chukchi Seas (Fig. 6E, Fig. 8B). North Pacific warming and stratification accompanied a crash in precipitation rates at Lake El'gygytgyn, coeval with a decrease in δD_{wax} values and gradual cooling (Fig. 5A, E, F, Fig. 8C). As at least some of the moisture reaching Lake El'gygytgyn today comes from the North Pacific, there must be another mechanism for reducing precipitation (and δD_P) at this time. We posit that the expansion of winter sea ice led to reduced precipitation at the lake and increased Raleigh distillation of precipitation en route, resulting in less latent heat export to interior Beringia (Fig. 8C). A change in the seasonality of precipitation (i.e. less summer precipitation) would also explain the isotopic change, but would not account for the crash in precipitation amount or cooling. During MIS G5, as the North Pacific reached a stable warm state, temperatures at Lake El'gygytgyn began to gradually rise due to increased sensible heat transport, while δD_{wax} remained unchanged (Fig. 5B, E, F). During MIS G5, we reconstruct a rapid enrichment of δD_{wax} followed by a marked increase in variability. We attribute this change to further establishment of sea-ice, perhaps extending into spring and fall (Fig. 8A). In addition, changing seasonality during MIS G3 may have contributed to the increased variability of δD_{wax} (Hennissen et al., 2015). We note that the shifts in δD_{wax} are coeval with the strengthening of North American dust sources, demonstrating clear linkages between land-ice and sea-ice occurring across iNHG (Naafs et al., 2012). Finally, beginning with MS G3, the amplitude of glacial–interglacial cycles in δD_{wax} and MBT/CBT increased due to both warmer interglacial and cooler glacial periods (Fig. 6H, I). This is consistent with expanding ice growth in the northern hemisphere (Shackleton et al., 1984; Kleiven et al., 2002), expansion of sea ice in the Arctic Basin (Knies et al., 2014), and increasing dominance of tundra vegetation at Lake El'gygytgyn (Brigham-Grette et al., 2013). Discrepancies between MBT/CBT and δD_{wax} throughout the record are a consequence of the different processes that affect the two proxies, especially difficult-to-constrain changes in vegetation and moisture sources that impact δD_{wax}.

5. Conclusions

The Lake El'gygytgyn terrestrial sequence documenting the transition of high northern latitudes from the warm Pliocene into the frequently glaciated Pleistocene is the first of its kind. Our application of the MBT/CBT palaeotemperature proxy captures glacial–interglacial temperature variability during the Pliocene–Pleistocene transition, demonstrating the potential for long-term environmental reconstruction using brGDGTs in the terrestrial Arctic. Cooling and drying are inferred coincident with major glaciation of the Northern Hemisphere during MIS G6. Temperature and vegetation change are closely linked, but vary independently of δD_{wax} for most the record. The δD_{wax} shows distinct shifts at 2.73 Ma (MIS G6) and 2.69 Ma (MIS G5), which we attribute to changes in moisture source and Raleigh distillation via the expansion of sea ice. Beginning with MIS 102, high-amplitude climate cycles are observed in MBT/CBT and δD_{wax}. We suggest this shift may represent a far-southern retreat of the treeline, expansion of land ice, and development of persistent sea-ice conditions similar to the Holocene. Existing pCO_2 records are not clearly linked with the terrestrial changes we reconstruct. This may be related to the resolution and precision of pCO_2 records, or may indicate that the carbon cycle, which has important high-latitude components (i.e. permafrost), had not fully synchronized with other parts of the climate system by MIS 95. Although insolation and pCO_2 are important drivers of ice-sheet expansion, these do not appear to be the sole drivers of Arctic environmental change during the Late Pliocene. Instead, our records suggest high-latitude climate feedbacks played a critical role in the intensification of Northern Hemisphere glaciation.

Acknowledgements

B.A.K. thanks Helen Habicht and Greg de Wet for useful feedback and discussions. Jeff Salacup is acknowledged for technical laboratory assistance. Norbert Nowaczyk, Volker Wennrich, and Martin Melles provided the age model tie points. We thank two anonymous reviewers and the editor for providing detailed comments that improved the manuscript and figures. This work was supported by National Science Foundation Grant No. 1204087, a NSF GRF to B.A.K. under Grant No. 1451512, and a Geological Society of America Graduate Student Research Grant. Drilling operations were funded by the International Continental Scientific Drilling Program, NSF, the German Federal Ministry of Education and Research, the Alfred Wegener Institute and Helmholtz Center Potsdam, the Far East Branch of the Russian Academy of Sciences, the Russian Foundation for Basic Research, and the Austrian Federal Ministry of Science and Research. Sample material used in this project, as well as sampling assistance, was provided by LacCore at the University of Minnesota. Data associated with this study are available on the NOAA National Centers for Environmental Information website.

Appendix A. Supplementary material

Supplementary material related to this article can be found online at http://dx.doi.org/10.1016/j.epsl.2016.09.058.

References

Andersson, R.A., Kuhry, P., Meyers, P., Zebühr, Y., Crill, P., Mörth, M., 2011. Impacts of paleohydrological changes on *n*-alkane biomarker compositions of a Holocene peat sequence in the eastern European Russian Arctic. Org. Geochem. 42, 1065–1075.

Andreev, A.A., Tarasov, P.E., Wennrich, V., Raschke, E., Herzschuh, U., Nowaczyk, N.R., Brigham-Grette, J., Melles, M., 2014. Late Pliocene and Early Pleistocene vegetation history of northeastern Russian Arctic inferred from the Lake El'gygytgyn pollen record. Clim. Past 10, 1017–1039.

Bailey, I., Hole, G.M., Foster, G.L., Wilson, P.A., Storey, C.D., Trueman, C.N., Raymo, M.E., 2013. An alternative suggestion for the Pliocene onset of major northern hemisphere glaciation based on the geochemical provenance of North Atlantic Ocean ice-rafted debris. Quat. Sci. Rev. 75, 181–194.

Ballantyne, A.P., Axford, Y., Miller, G.H., Otto-Bliesner, B.L., Rosenbloom, N., White, J.W., 2013. The amplification of Arctic terrestrial surface temperatures by reduced sea-ice extent during the Pliocene. Palaeogeogr. Palaeoclimatol. Palaeoecol. 386, 59–67.

Barr, I.D., Clark, C.D., 2011. Glaciers and climate in Pacific Far NE Russia during the Last Glacial Maximum. J. Quat. Sci. 26, 227–237.

Bischoff, J., Mangelsdorf, K., Schwamborn, G., Wagner, D., 2014. Impact of lake-level and climate changes on microbial communities in a terrestrial permafrost sequence of the El'gygytgyn crater, far east Russian arctic. Permafr. Periglac. Process. 25, 107–116.

Brigham-Grette, J., Carter, L.D., 1992. Pliocene marine transgressions of northern Alaska: circumarctic correlations and paleoclimatic interpretations. Arctic 45, 74–89.

Brigham-Grette, J., Melles, M., Minyuk, P., Andreev, A., Tarasov, P., DeConto, R., Koenig, S., Nowaczyk, N., Wennrich, V., Rosen, P., Haltia, E., Cook, T., Gebhardt, C., Meyer-Jacob, C., Snyder, J., Herzschuh, U., 2013. Pliocene warmth, polar amplification, and stepped pleistocene cooling recorded in NE Arctic Russia. Science 340, 1421–1427.

Bromwich, D.H., Toracinta, E.R., Wei, H., Oglesby, R.J., Fastook, J.L., Hughes, T.J., 2004. Polar MM5 simulations of the winter climate of the Laurentide Ice Sheet at the LGM. J. Climate 17, 3415–3433.

Buckles, L.K., Weijers, J.W., Verschuren, D., Damsté, J.S.S., 2014. Sources of core and intact branched tetraether membrane lipids in the lacustrine environment: anatomy of Lake Challa and its catchment, equatorial East Africa. Geochim. Cosmochim. Acta 140, 106–126.

Bush, R.T., McInerney, F.A., 2015. Influence of temperature and C_4 abundance on *n*-alkane chain length distributions across the central USA. Org. Geochem. 79, 65–73.

D'Anjou, R.M., Wei, J.H., Castañeda, I.S., Brigham-Grette, J., Petsch, S.T., Finkelstein, D.B., 2013. High-latitude environmental change during MIS 9 and 11: biogeochemical evidence from Lake El'gygytgyn, Far East Russia. Clim. Past 9, 567–581.

Dansgaard, W., 1964. Stable isotopes in precipitation. Tellus 16, 436–468.

de Wet, G.A., Castañeda, I.S., DeConto, R.M., Brigham-Grette, J., 2016. A high-resolution mid-Pleistocene temperature record from Arctic Lake El'gygytgyn: a 50 kyr super interglacial from MIS 33 to MIS 31? Earth Planet. Sci. Lett. 436, 56–63.

DeConto, R.M., Pollard, D., Wilson, P.A., Pälike, H., Lear, C.H., Pagani, M., 2008. Thresholds for Cenozoic bipolar glaciation. Nature 455, 652–656.

DeSchepper, S., Gibbard, P.L., Salzmann, U., Ehlers, J., 2014. A global synthesis of the marine and terrestrial evidence for glaciation during the Pliocene Epoch. Earth-Sci. Rev. 135, 83–102.

Dowsett, H., Dolan, A., Rowley, D., Pound, M., Salzmann, U., Robinson, M., Chandler, M., Foley, K., Haywood, A., 2016. The PRISM4 (mid-Piacenzian) palaeoenvironmental reconstruction. Clim. Past Discuss. 2016, 1–39.

Duk-Rodkin, A., Hughes, O.L., 1994. Tertiary-quaternary drainage of the Pre-glacial Mackenzie basin. Quat. Int. 22, 221–241.

Eglinton, G., Hamilton, R.J., 1967. Leaf epicuticular waxes. Science 156, 1322–1335.

Fedorov, G., Nolan, M., Brigham-Grette, J., Bolshiyanov, D., Schwamborn, G., Juschus, O., 2013. Preliminary estimation of lake El'gygytgyn water balance and sediment income. Clim. Past 9 (4), 1455–1465.

Foster, L.C., Pearson, E.J., Juggins, S., Hodgson, D.A., Saunders, K.M., Verleyen, E., Roberts, S.J., 2016. Development of a regional glycerol dialkyl glycerol tetraether (GDGT) – temperature calibration for antarctic and sub-antarctic lakes. Earth Planet. Sci. Lett. 433, 370–379.

Funder, S.V., Böcher, J., Bennike, O., Israelson, C., Petersen, K.S., Simonarson, L., 2004. Late Pliocene Greenland – The Kap København formation in North Greenland. Bull. Geol. Soc. Den., 117–134.

Gebhardt, A.C., Francke, A., Kück, J., Sauerbrey, M., Niessen, F., Wennrich, V., Melles, M., 2013. Petrophysical characterization of the lacustrine sediment succession drilled in Lake El'gygytgyn, Far East Russian Arctic. Clim. Past 9, 1933–1947.

Gibbard, P.L., Head, M.J., Walker, M.J.C., 2010. Formal ratification of the quaternary system/period and the Pleistocene series/epoch with a base at 2.58 Ma. J. Quat. Sci. 25 (2), 96–102.

Gualtieri, L., Brigham-Grette, J., 2001. The age and origin of the little diomede island upland surface. Arctic 54 (1), 12–21.

Haug, G.H., Ganopolski, A., Sigman, D.M., Rosell-Melé, A., Swann, G.E., Tiedemann, R., Jaccard, S.L., Bollmann, J., Maslin, M.A., Leng, M.J., 2005. North Pacific seasonality and the glaciation of North America 2.7 million years ago. Nature 433, 821–825.

Hennissen, J.A., Head, M.J., Schepper, S.D., Groeneveld, J., 2015. Increased seasonality during the intensification of Northern Hemisphere glaciation at the Pliocene–Pleistocene boundary, 2.6 Ma. Quat. Sci. Rev. 129, 321–332.

Holland, A.R., Petsch, S.T., Castañeda, I.S., Wilkie, K.M., Burns, S.J., Brigham-Grette, J., 2013. A biomarker record of Lake El'gygytgyn, Far East Russian Arctic: investigating sources of organic matter and carbon cycling during Marine Isotope Stages 1–3. Clim. Past 9, 243–260.

Hopmans, E.C., Schouten, S., Damsté, J.S.S., 2016. The effect of improved chromatography on GDGT-based palaeoproxies. Org. Geochem. 93, 1–6.

Hopmans, E.C., Schouten, S., Pancost, R.D., van der Meer, M.T., Sinninghe Damsté, J.S., 2000. Analysis of intact tetraether lipids in archaeal cell material and sediments by high performance liquid chromatography/atmospheric pressure chemical ionization mass spectrometry. Rapid Commun. Mass Spectrom. 14, 585–589.

Hu, A., Meehl, G.A., Han, W., Otto-Bliestner, B., Abe-Ouchi, A., Rosenbloom, N., 2015. Effects of the Bering Strait closure on AMOC and global climate under different background climates. Prog. Oceanogr. 132, 174–196.

Huybers, P.J., 2006. Early pleistocene glacial cycles and the integrated summer insolation forcing. Science 313, 508–511.

Kleiven, H.F., Jansen, E., Fronval, T., Smith, T.M., 2002. Intensification of Northern Hemisphere glaciations in the circum Atlantic region (3.5–2.4 Ma) – ice-rafted detritus evidence. Palaeogeogr. Palaeoclimatol. Palaeoecol. 184, 213–223.

Knies, J., Cabedo-Sanz, P., Belt, S.T., Baranwal, S., Fietz, S., Rosell-Melé, A., 2014. The emergence of modern sea ice cover in the Arctic Ocean. Nat. Commun. 5, 5608.

Lang, D.C., Bailey, I., Wilson, P.A., Chalk, T.B., Foster, G.L., Gutjahr, M., 2016. Incursions of southern-sourced water into the deep North Atlantic during late Pliocene glacial intensification. Nat. Geosci. 9, 375–379.

Laskar, J., Robutel, P., Joutel, F., Gastineau, M., Correia, A.C.M., Levrard, B., 2004. A long-term numerical solution for the insolation quantities of the Earth. Astron. Astrophys. 428, 261–285.

Layer, P.W., 2000. Argon-40/argon-39 age of the El'gygytgyn impact event, Chukotka, Russia. Meteorit. Planet. Sci. 35, 591–599.

Lisiecki, L.E., Raymo, M.E., 2005. A Pliocene–Pleistocene stack of 57 globally distributed benthic $\delta^{18}O$ records. Paleoceanography 20, PA1003.

Loomis, S.E., Russell, J.M., Heureux, A.M., D'Andrea, W.J., Damsté, J.S.S., 2014. Seasonal variability of branched glycerol dialkyl glycerol tetraethers (brGDGTs) in a temperate lake system. Geochim. Cosmochim. Acta 144, 173–187.

Loomis, S.E., Russell, J.M., Ladd, B., Street-Perrott, F.A., Damsté, J.S.S., 2012. Calibration and application of the branched GDGT temperature proxy on East African lake sediments. Earth Planet. Sci. Lett. 357 (358), 277–288.

Martínez-Botí, M.A., Foster, G.L., Chalk, T.B., Rohling, E.J., Sexton, P.F., Lunt, D.J., Pancost, R.D., Badger, M.P.S., Schmidt, D.N., 2015. Plio-Pleistocene climate sensitivity evaluated using high-resolution CO_2 records. Nature 518, 49–54.

Martínez-Garcia, A., Rosell-Melé, A., McClymont, E.L., Gersonde, R., Haug, G.H., 2010. Subpolar link to the emergence of the modern equatorial pacific cold tongue. Science 328, 1550–1553.

Melles, M., Brigham-Grette, J., Minyuk, P.S., Nowaczyk, N.R., Wennrich, V., DeConto, R.M., Anderson, P.M., Andreev, A.A., Coletti, A., Cook, T.L., Haltia-Hovi, E., Kukkonen, M., Lozhkin, A.V., Rosen, P., Tarasov, P., Vogel, H., Wagner, B., 2012. 2.8 million years of arctic climate change from Lake El'gygytgyn, NE Russia. Science 337, 315–320.

Meyers, S.R., 2012. Seeing red in cyclic stratigraphy: spectral noise estimation for astrochronology. Paleoceanography 27 (3), PA3228.

Meyers, S.R., 2014. Astrochron: An R Package for Astrochronology.

Miller, G., Brigham-Grette, J., Alley, R., Anderson, L., Bauch, H., Douglas, M., Edwards, M., Elias, S., Finney, B., Fitzpatrick, J., Funder, S., Herbert, T., Hinzman, L., Kaufman, D., MacDonald, G., Polyak, L., Robock, A., Serreze, M., Smol, J., Spielhagen, R., White, J., Wolfe, A., Wolff, E., 2010. Temperature and precipitation history of the Arctic. Quat. Sci. Rev. 29 (15–16), 1679–1715. Special theme: Arctic Palaeoclimate Synthesis (pp. 1674–1790).

Miller, K.G., Wright, J.D., Browning, J.V., Kulpecz, A., Kominz, M., Naish, T.R., Cramer, B.S., Rosenthal, Y., Peltier, W.R., Sosdian, S., 2012. High tide of the warm Pliocene: implications of global sea level for Antarctic deglaciation. Geology 40 (5), 407–410. http://dx.doi.org/10.1130/G32869.1.

Mock, C.J., Bartlein, P.J., Anderson, P.M., 1998. Atmospheric circulation patterns and spatial climatic variations in Beringia. Int. J. Climatol. 18, 1085–1104.

Naafs, B.D.A., Hefter, J., Acton, G., Haug, G.H., Martínez-Garcia, A., Pancost, R., Stein, R., 2012. Strengthening of North American dust sources during the late Pliocene (2.7 Ma). Earth Planet. Sci. Lett. 317–318, 8–19.

Niessen, F., Hong, J.K., Hegewald, A., Matthiessen, J., Stein, R., Kim, H., Kim, S., Jensen, L., Jokat, W., Nam, S.-I., Kang, S.-H., 2013. Repeated Pleistocene glaciation of the East Siberian continental margin. Nat. Geosci. 6, 842–846.

Nolan, M., Brigham-Grette, J., 2007. Basic hydrology, limnology, and meteorology of modern Lake El'gygytgyn, Siberia. J. Paleolimnol. 37, 17–35.

Nolan, M., Cassano, E.N., Cassano, J.J., 2013. Synoptic climatology and recent climate trends at Lake El'gygytgyn. Clim. Past 9, 1271–1286.

Nowaczyk, N.R., Haltia, E.M., Ulbricht, D., Wennrich, V., Sauerbrey, M.A., Rosen, P., Vogel, H., Francke, A., Meyer-Jacob, C., Andreev, A.A., Lozhkin, A.V., 2013. Chronology of Lake El'gygytgyn sediments: a combined magnetostratigraphic, palaeoclimatic and orbital tuning study based on multi-parameter analyses. Clim. Past 9, 2413–2432.

Pautler, B.G., Reichart, G.-J., Sanborn, P.T., Simpson, M.J., Weijers, J.W.H., 2014. Comparison of soil derived tetraether membrane lipid distributions and plant-wax δD compositions for reconstruction of Canadian Arctic temperatures. Palaeogeogr. Palaeoclimatol. Palaeoecol. 404, 78–88.

Peterse, F., van der Meer, J., Schouten, S., Weijers, J.W.H., Fierer, N., Jackson, R.B., Kim, J.-H., Damsté, J.S.S., 2012. Revised calibration of the MBT-CBT paleotemperature proxy based on branched tetraether membrane lipids in surface soils. Geochim. Cosmochim. Acta 96, 215–229.

Polissar, P.J., D'Andrea, W.J., 2014. Uncertainty in paleohydrologic reconstructions from molecular δD values. Geochim. Cosmochim. Acta 129, 146–156.

Poynter, J., Eglinton, G., 1990. Molecular composition of three sediments from Hole 717c: the Bengal fan. Proc. Ocean Drill. Program Sci. Results 116, 155–161.

Prescott, C.L., Haywood, A.M., Dolan, A.M., Hunter, S.J., Pope, J.O., Pickering, S.J., 2014. Assessing orbitally-forced interglacial climate variability during the mid-Pliocene Warm Period. Earth Planet. Sci. Lett. 400, 261–271.

Sachse, D., Billault, I., Bowen, G.J., Chikaraishi, Y., Dawson, T.E., Feakins, S.J., Freeman, K.H., Magill, C.R., McInerney, F.A., van der Meer, M.T.J., Polissar, P., Robins,

R.J., Sachs, J.P., Schmidt, H.-L., Sessions, A.L., White, J.W.C., West, J.B., Kahmen, A., 2012. Molecular paleohydrology: interpreting the hydrogen-isotopic composition of lipid biomarkers from photosynthesizing organisms. Annu. Rev. Earth Planet. Sci. 40, 221–249.

Schoon, P.L., de Kluijver, A., Middelburg, J.J., Downing, J.A., Damsté, J.S.S., Schouten, S., 2013. Influence of lake water pH and alkalinity on the distribution of core and intact polar branched glycerol dialkyl glycerol tetraethers (GDGTs) in lakes. Org. Geochem. 60, 72–82.

Schouten, S., Huguet, C., Hopmans, E.C., Kienhuis, M.V.M., Sinninghe Damsté, J.S., 2007. Analytical methodology for TEX_{86} paleothermometry by high-performance liquid chromatography/atmospheric pressure chemical ionization-mass spectrometry. Anal. Chem. 79, 2940–2944.

Shackleton, N.J., Backman, J., Zimmerman, H., Kent, D.V., Hall, M.A., Roberts, D.G., Schnitker, D., Baldauf, J.G., Desprairies, A., Homrighausen, R., Huddlestun, P., Keene, J.B., Kaltenback, A.J., Krumsiek, K.A.O., Morton, A.C., Murray, J.W., Westberg-Smith, J., 1984. Oxygen isotope calibration of the onset of ice-rafting and history of glaciation in the North Atlantic region. Nature 307, 620–623.

Shanahan, T.M., Hughen, K.A., Ampel, L., Sauer, P.E., Fornace, K., 2013a. Environmental controls on the 2H/1H values of terrestrial leaf waxes in the eastern Canadian Arctic. Geochim. Cosmochim. Acta 119, 286–301.

Shanahan, T.M., Hughen, K.A., Van Mooy, B.A.S., 2013b. Temperature sensitivity of branched and isoprenoid GDGTs in Arctic lakes. Org. Geochem. 64, 119–128.

Sun, Q., Chu, G., Liu, M., Xie, M., Li, S., Ling, Y., Wang, X., Shi, L., Jia, G., Lü, H., 2011. Distributions and temperature dependence of branched glycerol dialkyl glycerol tetraethers in recent lacustrine sediments from China and Nepal. J. Geophys. Res. 116, G01008.

Takahashi, K., Ravelo, A.C., Zarikian, C.A., Scientists, I.E., 2011. IODP Expedition 323 – Pliocene and Pleistocene paleoceanographic changes in the Bering Sea. Sci. Drill. 11, 4–13.

Thompson, R.S., Fleming, R.F., 1996. Middle Pliocene vegetation: reconstructions, paleoclimatic inferences, and boundary conditions for climate modeling. Mar. Micropaleontol. 27, 27–49.

Thomson, D.J., 1982. Spectrum estimation and harmonic analysis. Proc. IEEE 70 (9), 1055–1096.

Tierney, J.E., Russell, J.M., Eggermont, H., Hopmans, E.C., Verschuren, D., Damsté, J.S.S., 2010. Environmental controls on branched tetraether lipid distributions in tropical East African lake sediments. Geochim. Cosmochim. Acta 74, 4902–4918.

Tindall, J.C., Haywood, A.M., 2015. Modeling oxygen isotopes in the pliocene: large-scale features over the land and ocean. Paleoceanography 30, 1183–1201, 2014PA002774.

Weijers, J.W., Schefuß, E., Schouten, S., Damsté, J.S.S., 2007a. Coupled thermal and hydrological evolution of tropical Africa over the last deglaciation. Science 315, 1701–1704.

Weijers, J.W.H., Schouten, S., van den Donker, J.C., Hopmans, E.C., Sinninghe Damsté, J.S., 2007b. Environmental controls on bacterial tetraether membrane lipid distribution in soils. Geochim. Cosmochim. Acta 71, 703–713.

Wilkie, K.M.K., Chapligin, B., Meyer, H., Burns, S., Petsch, S., Brigham-Grette, J., 2013. Modern isotope hydrology and controls on δD of plant leaf waxes at Lake El'gygytgyn, NE Russia. Clim. Past 9, 335–352.

Woodard, S.C., Rosenthal, Y., Miller, K.G., Wright, J.D., 2014. Antarctic role in Northern Hemisphere glaciation. Science 346, 847–851.

Zhang, Y.G., Pagani, M., Liu, Z., Bohaty, S.M., DeConto, R., 2013. A 40-million-year history of atmospheric CO_2. Philos. Trans. R. Soc., Math. Phys. Eng. Sci. 371, 20130096.